View metadata, citation and similar papers at core.ac.uk
brought to you by CORE
provided by DSpace@MIT

PSFC/JA-04-14

Full Wave Simulations of Fast Wave Mode Conversion and Lower Hybrid Wave Propagation in Tokamaks

J.C. Wright, P.T. Bonoli, M. Brambilla, F. Meo, E. D'Azevedo,
D.B. Batchelor, E.F. Jaeger, L.A. Berry, C.K. Phillips, A. Pletzer

March 2004

Plasma Science and Fusion Center
Massachusetts Institute of Technology
Cambridge, MA 02139 USA

This work was supported by the U.S. Department of Energy, Grant No. DE-FC02-01ER-54648.

Physics of Plasmas (May 2004)

Full wave simulations of fast wave mode conversion and lower hybrid wave propagation in tokamaks[a]

J. C. Wright[b] and P. T. Bonoli
Massachusetts Institute of Technology, Plasma Science and Fusion Center, Cambridge, Massachusetts 02139

M. Brambilla and F. Meo
Max-Planck-Institut für Plasmaphysik, Euratom Association, Boltzmannstrasse 2, D-85748 Garching bei München, Germany

E. D'Azevedo, D. B. Batchelor, E. F. Jaeger, and L. A. Berry
P.O. Box 2009, Oak Ridge National Laboratory, Oak Ridge, Tennessee 37831-8071

C. K. Phillips and A. Pletzer
Princeton Plasma Physics Laboratory, Princeton, New Jersey 08543
(Dated: (Received 31 October 2003; accepted 2 January 2004))

Fast Wave (FW) studies of mode conversion (MC) processes at the ion–ion hybrid layer in toroidal plasmas must capture the disparate scales of the FW and mode converted ion Bernstein (IBW) and ion cyclotron waves (ICW). Correct modeling of the MC layer requires resolving wavelengths on the order of $k_\perp \rho_\mathrm{i} \sim 1$ which leads to a scaling of the maximum poloidal mode number, M_max, proportional to $1/\rho^*$ ($\rho^* \equiv \rho_\mathrm{i}/L$). The computational resources needed a scale with the number of radial (N_r), poloidal (N_θ), and toroidal (N_ϕ) elements as $\mathrm{N_r} * \mathrm{N}_\phi * \mathrm{N}_\theta^3$. Two full wave codes, a massively-parallel-processor (MPP) version of the `TORIC-2D` finite Larmor radius code [M. Brambilla, Plasma Phys. Controlled Fusion **41**, 1 (1999)] and also an all orders spectral code `AORSA2D` [E. F. Jaeger *et al.*, Phys. Plasmas **9**, 1873 (2002)], have been developed which for the first time are capable of achieving the resolution and speed necessary to address mode conversion phenomena in full two-dimensional (2-D) toroidal geometry. These codes have been used in conjunction with theory and experimental data from the Alcator C-Mod [I. H. Hutchinson *et al.*, Phys. Plasmas **1**, 1511 (1994)] to gain new understanding into the nature of FWMC in tokamaks. The MPP version of `TORIC` is also now capable of running with sufficient resolution to model planned lower hybrid range of frequencies (LHRF) experiments in the Alcator C-Mod.

I. INTRODUCTION

Until recently, memory and processor speeds of serial computers were insufficient to converge calculations of mode converted ion Bernstein wave fields in 2-D tokamak geometry using full wave spectral solvers in the ion cyclotron range of frequencies (ICRF.) The number of spectral modes used for the poloidal dimension have long been known to be inadequate because resolving the mode converted waves can be shown to require 300–1000 modes while typical simulations to date have used less than 100. We present results here using new out-of-core memory management and parallel algorithms that produce results that are demonstrably converged in resolution. New high resolution simulations of mode conversion electron heating experiments in the Alcator C-Mod show good agreement with experimental measurements over a wide range of minority species concentrations.

In toroidal plasmas, the relatively long wavelength fast magneto-sonic wave (FW) will mode convert to the much shorter electrostatic ion Bernstein wave (IBW)[1] and the intermediate wavelength slow electromagnetic ion cyclotron wave (ICW).[2] This mode conversion process occurs in a narrow mode-degenerate surface in the plasma known as the ion–ion hybrid layer that occurs in multi-ion species plasmas. Its location is determined by the magnetic field strength and by the concentration of the minority ion-species.[2] Direct control of the location of this process makes mode conversion of FWs a means of creating current drive, heating and modifying the plasma temperature and current density profiles, and a possible means for flow drive.[3]

In this paper, we use a toroidal full wave spectral code, `TORIC`,[4,5] to model this mode conversion process. As we shall show, the high wave-number of the IBW and the narrow vertical layer of the mode conversion surfaces in toroidal geometry impose significant resolution requirements. By implementing parallel algorithms in the `TORIC` code, we have been able to exceed these requirements and demonstrate clear numerical convergence of the spectral expansion. In Sec. II we describe the code and the addition of massively-parallel-processor (MPP) modifications. in Sec. III, we present applications to the Alcator C-Mod mode conversion and discuss the implications for other devices. In Sec. IV, we compare `TORIC` with the all orders full wave code, `AORSA-2D`,[6] to validate the truncated dielectric response used in `TORIC`. In Sec. V, initial steps toward modeling of lower hybrid waves with a full wave code are given. We give our summary and conclusion in Sec. VI.

---

[a]Paper GI 2 6, Bull. Am. Phys. Soc. **48**, 127 (2003).
[b]Invited speaker. Electronic mail: `jcwright@mit.edu`

II. CODE DESCRIPTION

A. Physics kernel

TORIC is a Finite Larmor Radius (FLR) Full Wave Code. "Full Wave" means that it solves Maxwell's equations in the presence of a plasma and wave antenna. It does this for a fixed frequency with a linear plasma response [Eq. (1a)] in a mixed spectral-finite element basis [Eq. (1b)]. Formally, the local plasma response is an integral function of the plasma volume [Eq. (1d)]. This may be seen easily by considering the oscillating plasma current as a moment of the perturbed particle distribution from the linearized Boltzmann equation in the presence of the electric field from the excited wave.[7] It is in this sense that TORIC has a linear plasma response. The linearity is exploited by transforming Maxwell's equations to frequency space, so that $d/dt \to -i\omega$. The TORIC code uses an FLR expansion to convert this vector integro-differential equation into a sixth order partial differential equation.[5,8] This approximation retains the second harmonic wave frequency and is second order in the ion gyro-radius, $(\rho_{\rm i} = v_{ti}/\Omega_{ci})$, for plasma interactions with the wave.

$$\nabla \times \nabla \times \mathbf{E} = \frac{\omega^2}{c^2}\left\{\mathbf{E} + \frac{4\pi i}{\omega}\left(\mathbf{J}^{\rm P} + \mathbf{J}^{\rm A}\right)\right\} \quad (1a)$$

$$\mathbf{E}(\mathbf{x}) = \sum_m \mathbf{E}_m(r)\exp\left(im\theta + in\phi\right) \quad (1b)$$

$$k_\parallel = \frac{m}{r}\frac{B_\theta}{B} + \frac{n_\phi}{R}\frac{B_\phi}{B} \quad (1c)$$

$$\mathbf{J}^P_m(r) = \sum_m \sigma_c\left(k^m_\parallel, r\right)\cdot\mathbf{E}_m(r) \quad (1d)$$

Here $\mathbf{J}^A$ and $\mathbf{J}^P$ are the antenna and plasma currents and σ_c is the plasma conductivity. Note that $\mathbf{J}^P$ is the oscillating current driven by the plasma wave and is distinct from the current induced in the electrons during current drive experiments that contributes toward the confining magnetic field. The antenna model presently in TORIC includes a Faraday shield, a scrape-off layer, and a vacuum region between the antenna and the wall of the vacuum chamber. It does not include three-dimensional effects such as the perpendicular current in the antenna feeders.

The integral plasma current response is expressed using the Swanson–Colestock–Kashuba[9,10] approximation, which retains only the FLR terms resonant at the second ion cyclotron frequency, $\omega = 2\Omega_{ci}$. While the approximation to the integral plasma current response is done to second order in the normalized perpendicular wavenumber, $k_\perp\rho_{\rm i}$, the damping for the IBW is good to all orders. This is done by modifying the imaginary part of the plasma dispersion to account for the IBW damping, while leaving the real part unchanged[8].

$$(n^2_\perp)_{\rm IBW} = -\frac{n^2_\parallel - S}{\sigma} \quad (2a)$$

$$\sigma \to \sigma + \delta\sigma \quad (2b)$$

$$\delta\sigma = -i\sigma\frac{{\rm Im}\{(n^2_\perp)_{\rm IBW}\}}{(n^2_\perp)_{\rm IBW}}. \quad (2c)$$

Equation (2a) describes the mode conversion of fast waves to either ion Bernstein waves or ion cyclotron waves at the ion–ion hybrid layer ($n^2_\parallel = S$) in a warm plasma,[4] where $\mathbf{n} \equiv \mathbf{k}c/\omega$ is the index of refraction. The warm plasma contribution, σ (not to be confused with the plasma conductivity, σ_c), is modified as shown in Eq. (2), in which a contribution derived from the $k_\perp$ root of the full local dispersion relation, $D(k_\parallel, k_\perp, \omega) = 0$, retaining all cyclotron harmonics[4], is added to the expression for the perpendicular wave number. At the point where this damping is significant, *e.g.* in the vicinity of the mode conversion layer, the perpendicular wavelength is very small, and the local dispersion relation applies. The important point of Eq. (2) is that since $|\delta\sigma| \ll |\sigma|$, the real dispersion will not be affected while the damping will be correct for large values of $k_\perp\rho_{\rm i}$.

In the actual implementation in the code, the perpendicular index of refraction, $n_\perp$, is present only as an operator. That is, $n_\perp \to (c/\omega)\nabla_\perp$, but the warm plasma effects are retained in σ as are the damping modifications to it in Eq. (2c). However, the spectral basis in Eq. (1b) does provide an analytic expression for the parallel wavenumber as given in Eq. (1c), and an easy bridge to the tools of homogeneous plasma wave theory. Because the poloidal modes are not of a local extent in θ within a flux surface, this basis set requires more terms to represent discontinuities such as mode conversion layers than a basis of finite extent such as wavelets would need. Resolution requirements depend on the specific wave scenario being modeled, and to an extent, on the type of basis being used.

B. Numerical model and parallel algorithm

The amount of resolution needed is also increased by wave dispersion. Shorter wavelength modes will need more radial and poloidal elements. In the case of mode conversion, the presence of IBW implies that the perpendicular wave number is on the order of the ion Larmor radius. From the condition that $k_\perp\rho_{\rm i} \simeq 1$, and approximating $k_\perp \sim m/r$, we may estimate the maximum poloidal mode number needed in the simulation by specifying the minor radius location of the mode conversion layer. In the Alcator C-Mod, $M_{\rm max} \simeq 173$, given a mode conversion layer at $r/a = 0.5$ in a deuterium plasma with a central field of 7.85 T and ion temperature of 1.8 keV. In the lower hybrid range of frequencies (LHRF), $(\Omega_e \gg \omega \gg \Omega_{\rm i})$, dispersion now yields: $(\omega_{\rm pe}/\omega)k_\parallel \sim k_\perp \sim m/r \Rightarrow M_{\rm max} \simeq 1000$, which is far in excess of what has been possible in the past. The resolution requirements found from simple dispersion relation arguments may be recast in terms of the familiar turbulence scaling parameter, $\rho^* \equiv \rho_{\rm i}/L$, where L is the scale of the device, so that, for IBW, $M_{\rm max} \sim 1/\rho^*$. This has important implications for simulating mode conversion and current drive in the next generation of fusion devices in which scalelengths will be significantly larger.

The discretization of the system of equations in Eqs. (1) leads to a block tri-diagonal system with $3 \times N_r$ blocks. A weak formulation of the equations is used with cubic Hermite polynomials in the radial dimension, which for the FLR system, creates a sparse block tri-diagonal structure. The

Fourier decomposition decouples the toroidal dimension for axisymmetric devices so that it only enters parametrically as the toroidal mode number, n_ϕ. Multiple simulations at different toroidal modes can be used to build up a complete three-dimensional spectrum. The poloidal modes are coupled by the free space operators and the plasma response and create dense blocks which contain $(2 \times 3 \times N_m)^2$ elements (for the real and imaginary parts of the three vector components.) Thus, the computational resources to solve for the fields quickly exceed the available memory of a single processor. For example, given an available memory of 2 Gigabytes of RAM, we would be limited to a maximum of approximately 150 radial elements by 128 poloidal modes, which is insufficient for the problems discussed above.

Prior to any enhancements to the code, the maximum problem size was 161 poloidal modes and 240 radial modes on one processor of the SV1 CRAY at NERSC, requiring 4 Gbyte of RAM and 10 cpu hours/toroidal mode. Several serial modifications were made to the code before parallelization. The matrix inversion is performed with the Thomas algorithm[11,12], which is just Gaussian inversion specialized to a tridiagonal system. We implemented an out of core solver that uses local scratch disks to store inverted matrix blocks during inversion in the Thomas algorithm. Though this technique requires that disks be local to be efficient, it greatly reduces in core memory requirements - by a factor of 25 for $N_m = 161, N_\mathrm{r} = 240$. Calculations in the power reconstruction were also converted to equivalent convolutions using fast Fourier transforms (FFT)s. These enhancements extended the problem size to 255 poloidal modes on one 1.4 GHz Athlon processor, requiring 2 Gbyte of RAM and 9.5 cpu hours/toroidal mode.

That resolution is barely sufficient to resolve some mode conversion scenarios in the Alcator C-Mod (see Sec. III). To achieve numerical convergence and to resolve mode conversion in larger machines or in cases where the hybrid layer lies at large minor radii, requires more resolution than can fit on a single processor machine. To take advantage of scalable architectures, the code has been parallelized as described in detail in Wright *et al.*[13] in the power reconstruction and the matrix inversion by using the ScaLAPACK[14] (Scalable Linear Algebra PACKage) library of parallelized linear algebra routines as well as direct use of the message passing interface (MPI). The out of core solver is still used, only now, the individual blocks are distributed across all the processors, and local scratch disks store parts of the inverted blocks. ScaLAPACK instead of LAPACK[14] is now used to perform the factorization into lower and upper triangular matrices (LU decompositions) and matrix-vector multiplies. In this way, the limiting memory requirements of the large blocks of the block diagonal system are distributed across multiple processors, and so the problem size is limited in principle only by the available number of processors. The speed up from this process is such that the power and current reconstructions become the dominant part of the elapsed run time. Since these reconstructions are independent of the flux surface dimension, it is the natural dimension along which to parallelize. After the solution of the wave fields is constructed and distributed among the processors, MPI calls are used to separate the power reconstructions into $\mathrm{n_p}$ (the number of processors) domains, which then proceed independently. Then MPI is used to collect the domains into vectors and arrays for output. This speed-up is linear with the number of processors, and reduces the time elapsed in the power reconstruction to an insignificant amount (*e.g.* less than 1% for the largest problems presented here.) The final result of the performance increase is shown in Table I.

TABLE I: A nonrigorous comparison of serial and parallel run times. The dashed time entry does not fit on one serial processor. Note that `TORIC` can now run with 255 modes in under an hour, while less resolution in the past took 10 hours on one vector Cray processor. As we shall show in Sec. III, that amount of resolution is sufficient for mode conversion studies in the Alcator C-Mod.

$\mathbf{N_m}$	**161**	255	511	**255**	511	1023
$\mathbf{N_r}$	**240**	240	240	480	480	480
Time(hrs)	**10**	9.5	—	**0.82**	3.6	25.5
Mach.(#pc)	K[a](1)	M[b](1)	M(1)	M(32)	M(32)	M(48)

[a]Killeen(K) is the Nersc k-machine with SV1 Cray vector processors (retired in 1997).

[b]Marshall(M) is the PSFC-MIT theory Beowulf cluster, comprised of 24, 2 GB 1.2 GHz dual Athlon processors.

III. CONVERGENCE STUDY FOR D(^{3}HE) MODE CONVERSION IN THE ALCATOR C-MOD

Alcator C-Mod is a compact ($R_0 = 0.67$ m, $a = 0.22$ m), high density, high magnetic field tokamak[15] that operates with ICRH as its only source of external heating. Mode conversion studies on C-Mod have been modeled in the past[16] by the `TORIC` code, but those simulations were reported to have had insufficient resolution for the range of parameters considered. In particular, these scenarios involved a high central magnetic field [$B(0) = 7.9T$] in a deuterium plasma with a minority of Helium-3 (^{3}He) that was varied in concentration. As the ^{3}He concentration is increased, more resolution is needed to resolve the narrowing separation between the ^{3}He fundamental cyclotron layer located approximately at the magnetic axis and the ion–ion hybrid layer to its left on the high field side. Figure 1 depicts the results of a resolved MC simulation for the case under consideration. An important feature of this plot is the narrow horizontal extent of the mode conversion layer and the short wavelength IBW to its left in the midplane. These two features make this case difficult to resolve.

We begin with a convergence study to demonstrate the need for high resolution to validate the poloidal spectral expansion. For a ^{3}He concentration of 24%, the MC layer and the ^{3}He fundamental layer are separated by approximately 7 cm. In Wright *et al.*,[13] we have shown graphically in[13] two-dimensional field plots how at low resolution, the excitation of the fields at the MC layer is not localized within the layer but follows the flux surface geometry around toward the the low field side to the ^{3}He resonance where it causes spurious ^{3}He power deposition. In Figs. 2 and 3, the increase of resolution

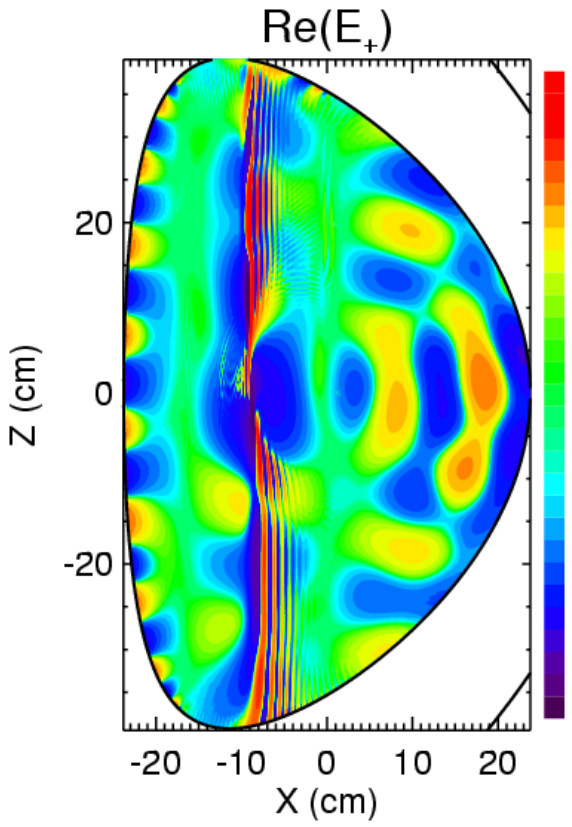

FIG. 1: TORIC simulation of a D(^{3}He) MC case in the Alcator C-Mod ($N_m = 511$ $N_\psi = 480$, $B_0 = 7.9$ T, $n_{^3\mathrm{He}}/n_\mathrm{e} = 0.24$). Note the well resolved presence of the midplane IBW propagating to the left, the ICW above and below the midplane going the the right, and large FW propagating from the right to the layer, with a small amount transmitting through.

from $N_m = 127$ to $N_m = 255$ poloidal modes demonstrates the need of the spectral expansion for a large number of modes to adequately resolve the MC layer. Note also that the outermost surface in the plot for $N_m = 255$ retains the most energy in the highest poloidal modes. This is because the MC layer extends vertically across the entire plasma and the poloidal mesh spacing is largest at the outermost flux surface.

TABLE II: The convergence of power deposition with poloidal resolution. The power is measured in percent of incident power. (The power to deuterium and hydrogen ion species is not shown.) The deuterium plasma has 5% minority hydrogen and 25% minority ^{3}He with a central magnetic field of 7.85 T, density of 2.4×10^{14} cm^{-3} and current of 1190 kA. Radial resolution of $N_r = 240$ for all cases.

N_m	15	31	63	127	161	255	511	1023[a]
ELD	20.2	14.9	23.0	50.0	55.4	77.4	90.2	93.4
^{3}He	65.6	71.1	67.7	44.7	38.0	17.4	6.3	4.9

[a]The 1023 case has 1% H instead of 5% H to shift a shear Alfvén resonance out of the scrape-off layer.

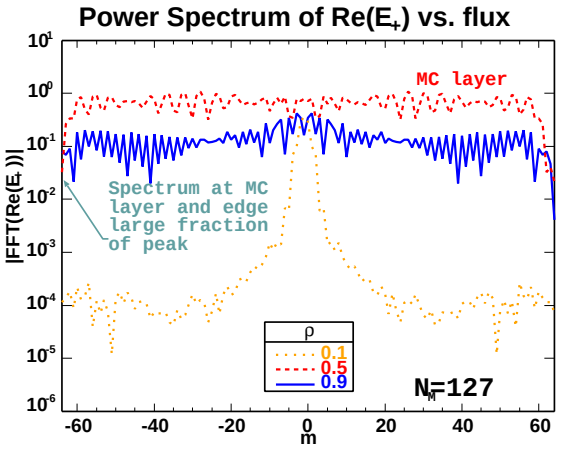

FIG. 2: Spectral convergence for a MC scenario with TORIC ($N_m = 127$). Fourier decompositions for three flux surfaces are shown with for insufficient poloidal resolution. The MC midplane surface at $\rho = 0.5$ and the outermost surface shown at $\rho = 0.9$ are clearly not well resolved.

As resolution is increased, the features of the converged MC layer apparent in Fig. 1 appear qualitatively at around $N_m = 161$ modes. However, by looking at the global power balances between electrons and ^{3}He, in Table II, we can see that convergence requires $N_m = 511$, in agreement with Fig. 3. Note that the converged case has the opposite power partition for electrons and ions than the low resolution case. Specifically, the simulations change their prediction from a majority of ion to a majority of electron heating. This also has an impact on modeling of MC physics on the C-Mod experiment. It has been shown in Ref. 17 that the results of Ref. 16 are improved by increasing the poloidal resolution to $N_m = 255$ poloidal modes. Figure 4 shows how the higher resolution studies follow the scaling of the experimental data with ^{3}He concentration, while the lower resolution fails to capture the increased electron damping as the ^{3}He concentration increases and the separation of the ion–ion hybrid layer and the ^{3}He fundamental cyclotron layer increases. One possible cause of the overshoot in the higher resolution cases at large ^{3}He concentration is the decreasing single pass absorption caused by the larger evanescent region between the cyclotron layer and MC layer. This results in multiple reflections off the boundaries during which parasitic processes such as a edge shear Alfvén resonance may absorb power. These processes are not modeled by the TORIC code.

IV. VALIDATION WITH ALL ORDERS MODEL FOR D–H–^{3}HE

In the previous section, we demonstrated that the FLR full wave code, TORIC, with a model for enhanced damping of short wavelength modes will converge when simulating mode conversion of the fast wave to ion Bernstein waves and ion cyclotron waves. The improved agreement with experiment shown in Ref. 17 serves as some validation of the model, but one would like to compare against a model that makes

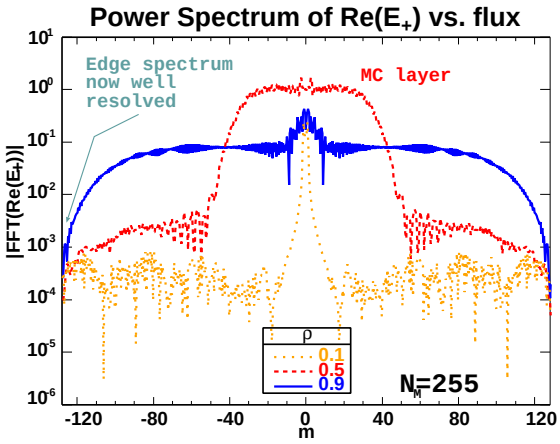

FIG. 3: Spectral convergence for a MC scenario with TORIC ($N_m = 255$). Fourier decompositions for three flux surfaces are shown with sufficient poloidal resolution. The MC midplane surface has responded strongly to the higher resolution and is converged to within the numerical noise floor.

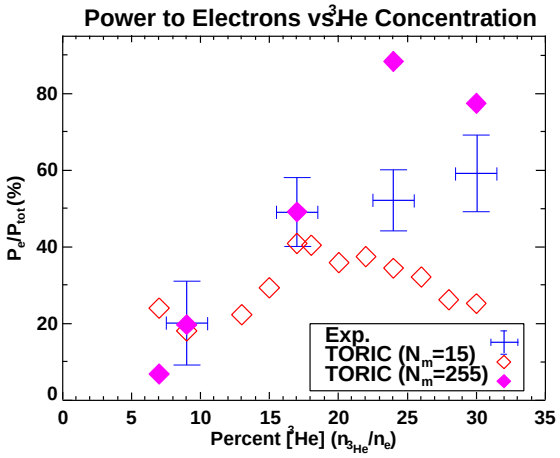

FIG. 4: D(^{3}He) mode conversion electron heating in the Alcator C-Mod (B_0 = 7.85 T, f_0 = 80 MHz). Volume integrated electron absorption versus ^{3}He density. The cross symbols with error bars are experimental data averaged over multiple rf power transitions. Open diamond symbols are TORIC simulations at lower resolution ($N_m = 15$), and the solid diamond symbols are TORIC simulations at high resolution ($N_m = 255$).

no approximations to the dielectric or the damping. The **A**ll **OR**ders **S**pectral **A**lgorithm (AORSA) code[6] retains all orders in $k_\perp \rho_\mathrm{i}$ in the plasma response, $\mathbf{J}^\mathrm{P} = \int \sigma_c(x,x') \cdot \mathbf{E}(x)$. It computes the solution to Eq. (1a) for toroidal systems in a cylindrical geometry with a fully spectral decomposition,

$$\mathbf{E}(x,y,\phi) = \sum_{n,m,l} \mathbf{E}_{n,m,l} \exp\left(i(k_n x + k_m y + l\phi)\right).$$

This fully spectral approach facilitates implementing the all orders conductivity, but results in a fully dense matrix, as compared to TORIC's matrix in which only a fraction of $(3/N_\mathrm{r})$ are nonzero. AORSA is a fully parallel code, and uses approximately 500 processors to hold this matrix for mode conversion simulations [in contrast, TORIC can do the same problem on as few as 8 processors (1 GB RAM 1.3 GHz IBM Power4 processors on the Cheetah[20] Oak Ridge computer)].

To eliminate any other sources of difference in the comparison, both codes use the same reconstructed EFIT equilibrium from an Alcator C-Mod discharge with a mixture of D–^{3}He–H in (21%–23%–33%) of n_e proportion, as well as the same temperature and density profiles. We first look at the mode conversion region as simulated by the two codes. In Fig. 5 we see that the two codes have nearly identical representations of the ICW above and below the midplane. The TORIC results do show an IBW propagating for about five wavelengths to the left of the MC layer in the midplane. This is consistent with one-dimensional modeling of this case by the one-dimensional model of AORSA and also by the one-dimensional code, METS95.[16,18] However, the AORSA-1D result required approximately twice the horizontal resolution ($N_x = 500$) to converge as the AORSA-2D results shown here. Presently, the maximum problem size is limited to the case shown. Larger cases will be possible over the course of the next year as new algorithms are implemented in AORSA, allowing a converged AORSA-2D simulation of this case.

Though the IBW wave accounts only for about 1% of the deposited power in this case, the global power balances for AORSA and TORIC differ significantly: TORIC- 77% P(e) 22% P(H) and AORSA- 51% P(e) 47% P(H). Again, from the 1-D results, we expect a majority of electron heating, but the differences in the two results cannot be explained by IBW damping. The difference lies in the ICW damping. Figure 6 shows TORIC's results for the entire cross-section. In the upper half in the area of $Z = [10, 22]$ cm, $X = 6$ cm, the ICW propagates quite close to the fundamental hydrogen cyclotron resonance layer. The reason for the clear up-down asymmetry of the ICW propagation is due to the poloidal dependence[3] of $k_\parallel$ as shown in Eq. (1c). ICW traveling clockwise have a negative poloidal mode number and so their $k_\parallel$ decreases as they propagate, corresponding to a smaller $\mathrm{Im}(k_\perp)$ and weaker damping. The counter-clockwise traveling ICW in the lower half have positive poloidal mode numbers, increasing $k_\parallel$, and larger $\mathrm{Im}(k_\perp)$, and so damp sooner. If there is insufficient resolution, the fields cause spurious damping on the hydrogen resonance, instead of electron Landau damping (ELD) on the electrons. This is seen clearly in resolution scans of TORIC (see Table II). At lower resolution in TORIC, the ELD in this region is reduced, and instead we see increased ion damping. This area is of additional interest because the amount of energy that does truly get coupled to the ions through the propagation of the downshifted ICW determines the strength of the force on the ions for flow drive.[3]

V. FAST WAVE SIMULATIONS IN THE LHRF REGIME

TORIC has been run in the ICRF regime with a resolution of $N_m = 1023 \times N_\psi = 480$, and this is sufficient to resolve the slow electrostatic LH wave. In order to take advantage of this resolution capability, the conductivity operator has been

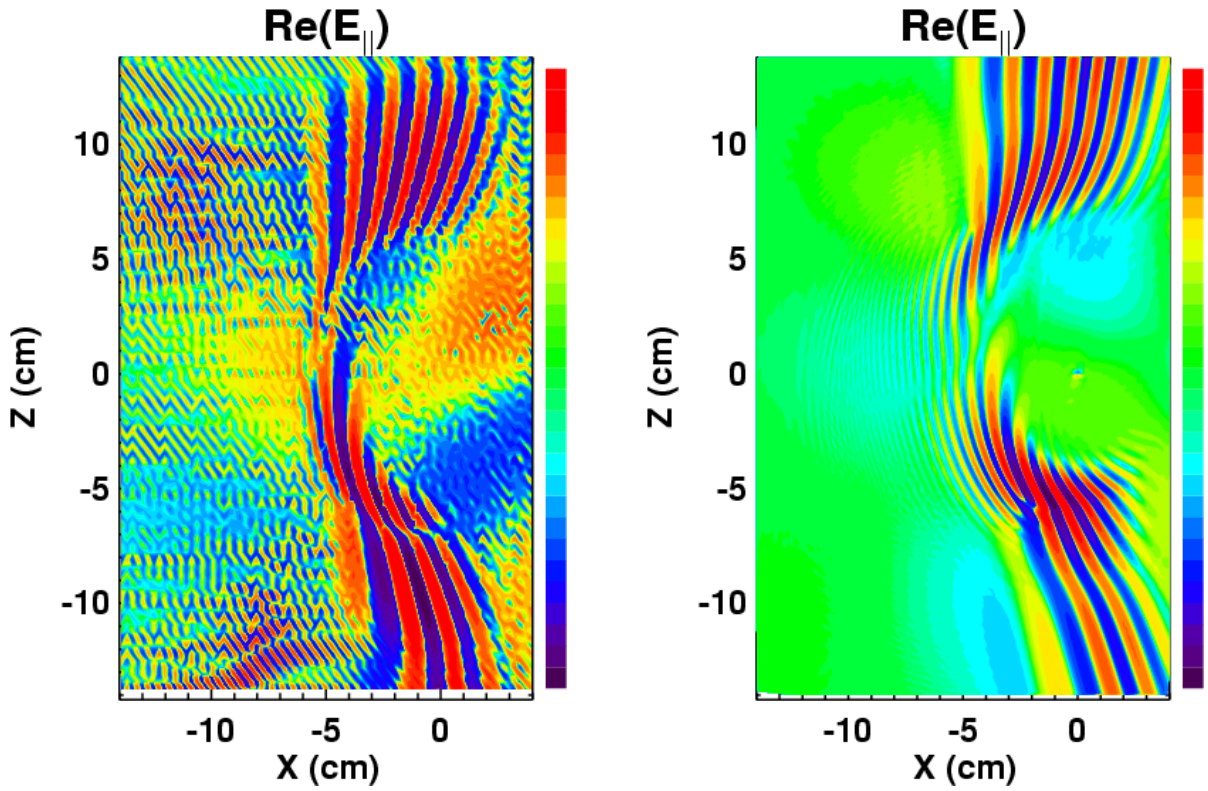

FIG. 5: The left panel shows an AORSA-2D simulation with a resolution of $230N_x \times 230N_y$. The right panel shows a TORIC simulation at $240N_\psi \times 255N_\theta$ resolution.

rewritten to be valid in the lower hybrid range of frequencies ($\Omega_{ci}^2 \ll \omega^2 \ll \Omega_{ce}^2$.) This corresponds to the limit of unmagnetized ions [$(k_\perp \rho_{\rm i})^2 \rightarrow \infty$] and strongly magnetized electrons [$(k_\perp \rho_e)^2 \ll 1$.] Presently the code couples to the FW polarization in the LHRF regime because only $E_\parallel = 0$ is permitted at the antenna.

Using this new dielectric formulation and the existing antenna model, TORIC has been used to resolve for the first time in toroidal geometry a lower hybrid fast wave. In Fig. 7 and Fig. 8, we show the results of these simulations. The parameters used were: $f_0 = 4.6$ GHz, n_ϕ=240, a=0.21 m, R_0=0.67 m, $B_0 = 5.3$ T, $n_\parallel = 2.7$, $T_{e0} = 3.5$ keV, and $T_{i0} = 2.0$ keV in a deuterium plasma. The two-dimensional positively polarized electric field in Fig. 7 shows the short FW wavelength at these frequencies as well as the effect of the FW cutoff on the high field side to the left of $X = 0$ in the contour plot. The power deposition profile in Fig. 8 is consistent with the LHRF fast wave in that the electron damping strength follows the plasma beta and shifts as the central electron temperature is changed. The modulation seen in the power deposition in Fig. 8, corresponds to the approximate 1 cm perpendicular wavelength of the lower hybrid fast wave.

VI. CONCLUSIONS

A new parallel algorithm has been implemented in the TORIC full wave ICRF code. Well converged simulations of mode-conversion scenarios are now possible and provide an important component in a current and flow drive physics model. An integrated model comprised of a fast full wave solver and Fokker–Planck solver for either electrons or ions could be used to study current or flow drive profile control via mode converted waves. Transport and turbulence codes could be added to evaluate the effects of the modified profiles on confinement and stability. Advanced scenarios in burning plasma devices such as the International Thermonuclear Experimental Reactor (ITER)[19] can now be modeled with the new resolution capabilities. The increased speed of the new parallel algorithms permits coupling to other codes to study a variety of physics problems such as antenna coupling, the effects of MC waves on transport, and quasilinear wave particle interactions (Fokker-Planck effects.) Furthermore, TORIC now has sufficient resolution and the proper dielectric implementation for lower-hybrid full wave simulations. Work is underway to modify the boundary conditions to couple to the slow wave ($E_\parallel \neq 0$ at the antenna.) Problems such as the role of wave focusing and diffraction in LH spectral broadening may yield new physics insights within the full wave framework.

ACKNOWLEDGMENTS

We would like to thank Dr. Stephen Wukitch, Dr. Yijun Lin, and Professor Miklos Porkolab for many enlightening discussions during the course of this work.

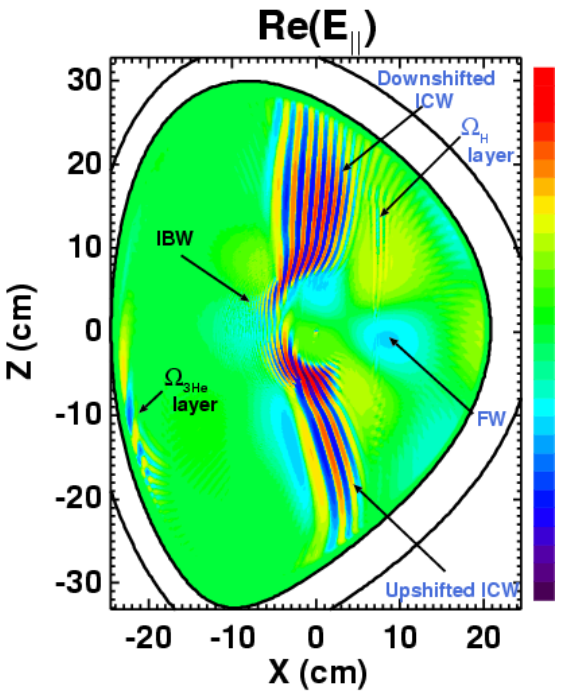

FIG. 6: Converged TORIC simulation of an Alcator C-Mod discharge a with mixture of D–^{3}He–H in (21%–23%–33%). The entire cross-section is shown. The ICW in the upper half propagates further than the ICW in the lower half because of the shift in $k_{\|}$.

This research has been sponsored by the Mathematical, Information, and Computational Sciences Division; Office of Advanced Scientific Computing Research; U.S. Department of Energy (DOE), under Contract No. DE-AC05-00OR22725 with UT-Battelle, LLC; and the DOE Wave–Particle Scidac (Scientific Discovery through Advanced Computing) Contract No. DE-FC02-01ER54648.

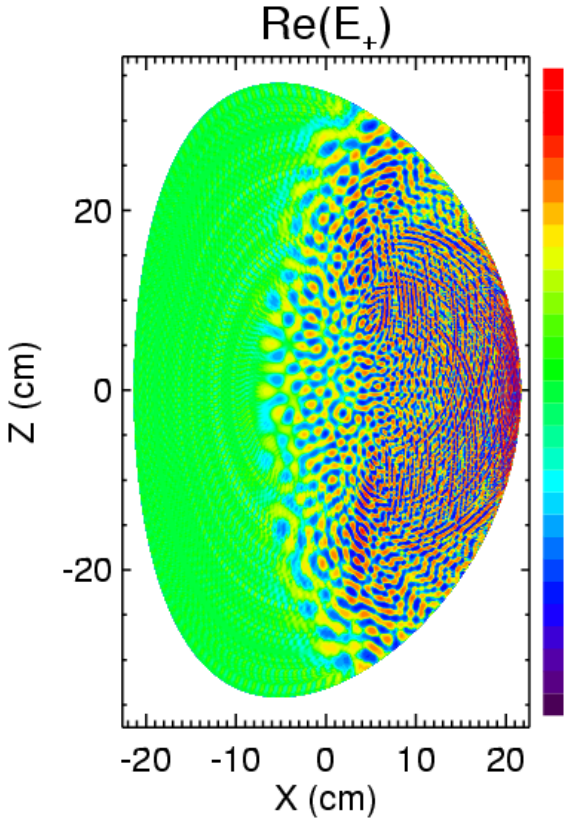

FIG. 7: TORIC simulation of a FW LH case in the Alcator C-Mod ($N_m = 255$ $N_\psi = 480$, $f_0 = 4.6$ GHz, n_ϕ=240, $B_0 = 5.3$ T, $n_{\|} = 2.7$, $T_{e0} = 3.5$ keV). Note the characteristic wavelength of a few millimeters, compared to the usual few centimeters at typical FW frequencies of 160 MHz.

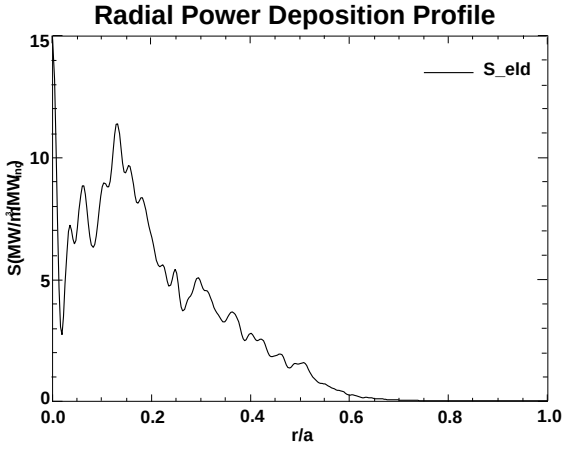

FIG. 8: The radial electron power deposition profile for a fast lower hybrid wave using Alcator C-Mod parameters ($f_0 = 4.6$ GHz, n_ϕ=240, $B_0 = 5.3$ T, $n_{\|} = 2.7$, $T_{e0} = 3.5$ keV).

[1] I. B. Bernstein, Phys. Rev. **109**, 10 (1958).

[2] F. W. Perkins, Nucl. Fusion **17**, 1197 (1977).

[3] E. F. Jaeger, L. A. Berry, J. R. Myra, D. B. Batchelor, E. D'Azevedo *et al.*, Phys. Rev. Lett. **90**, 195001 (2003).

[4] M. Brambilla, Nucl. Fusion **38**, 1805 (1998).

[5] M. Brambilla, Plasma Phys. Controlled Fusion **41**, 1 (1999).

[6] E. F. Jaeger, L. A. Berry, E. D. Azevedo, D. B. Batchelor, M. D. Carter *et al.*, Phys. Plasmas **9**, 1873 (2002).

[7] T. H. Stix, *The Theory of Plasma Waves* American Institute of Physics, New York, 1992 , Chap. 10, p. 250.

[8] M. Brambilla, and T. Krücken, Nucl. Fusion **28**, 1813 (1988).

[9] D. G. Swanson, Phys. Fluids **24**, 2035 (1981).

[10] P. T. Colestock, and R. J. Kashuba, Nucl. Fusion **23**, 763 (1983).

[11] W. F. Ames, *Numerical Methods for Partial Differential Equations* Academic Press, New York, 1977 , 2nd ed.

[12] G. H. Bruce, D. W. Peaceman, H. H. Rachford, and J. D. Rice., Trans. Am. Inst. Min., Metall. Pet. Eng. **198**, 79 (1953).

[13] J. C. Wright, P. T. Bonoli, E. D. Azevedo, and M. Brambilla, in *The 18th International Conference on Numerical Simulation of Plasmas September 7-10, 2003, CapeCod, Falmouth, Massachusetts, USA* Computer Phys. Comm., 2003 .

[14] J. Choi, J. J. Dongarra, L. S. Ostrouchov, A. P. Petitet, D. W. Walker *et al.*, Scientific Programming **5**, 173 (1996).

[15] I. H. Hutchinson *et al.*, Phys. Plasmas **1**, 1511 (1994).

[16] P. T. Bonoli, M. Brambilla, E. Nelson-Melby, C. K. Phillips, M. Porkolab *et al.*, Phys. Plasmas **7**, 1886 (2000).

[17] J. C. Wright, P. T. Bonoli, E. D. Azevedo, and M. Brambilla, in *Proceedings of the 15th Conference on Radio Frequency Power in Plasmas*, edited by C. B. Forest American Institute of Physics, New York, 2003 , No. 694, pp. 511–514.

[18] D. N. Smithe, C. K. Phillips, J. C. Hosea, R. P. Majeski, and J. R. Wilson, in *Proceedings of the 12th Topical Conference on Radio Frequency Power in Plasmas (in Savannah, GA)* AIP Conf. Proc., 1997 , No. 403, p. 367.

[19] ITER Physics Expert Group on Energetic Particles, Heating and Current Drive and ITER Physics Basis Editors, Nucl. Fusion **39**, 2495 (1999).

[20] Center for Computational Sciences at Oak Ridge National Laboratory, which is supported by the Office of Science of the U.S. Department of Energy under Contract No. DE-AC05-00OR22725